

# Lattice QCD study on $K^*(892)$ meson decay width

Ziwen Fu<sup>1,\*</sup> and Kan Fu<sup>2,†</sup>

<sup>1</sup> *Key Laboratory of Radiation Physics and Technology (Sichuan University), Ministry of Education; Institute of Nuclear Science and Technology; College of Physical Science and Technology, Sichuan University, Chengdu 610064, P. R. China.*

<sup>2</sup> *School of Environment, Tsinghua University, Peking 100084, P. R. China.*

(Dated: August 17, 2018)

We deliver an exploratory lattice QCD examination of the  $K^*(892)$  meson decay width with the help of the  $p$ -wave scattering phase  $\delta_1$  of pion-kaon ( $\pi K$ ) system in the isospin  $I = 1/2$  channel, which is extracted by the modified Rummukainen-Gottlieb formula for two-particle system with arbitrary masses, and it clearly reveals the entity of a resonance at a mass around  $K^*(892)$  meson mass. The effective range formula is applied to describe the energy dependence of scattering phase and we obtain the effective  $K^* \rightarrow \pi K$  coupling constant as  $g_{K^*\pi K} = 6.38(78)$ , and subsequently achieve the decay width as  $\Gamma_{K^*} = 64.9 \pm 8.0$  MeV, which is in reasonable accordance with the experiment. Our lattice investigations are conducted on a  $20^3 \times 48$  MILC full QCD gauge configuration at  $(m_\pi + m_K)/m_{K^*} \approx 0.739$  and the lattice spacing  $a \approx 0.15$  fm.

PACS numbers: 12.38.Gc, 11.15.Ha

## I. INTRODUCTION

It is well-known that the vector  $K^*(892)$  meson is a resonance. In 2012, the Particle Data Group (PDG) listed the  $K^*(892)$  meson  $I(J^P) = \frac{1}{2}(1^-)$ , with a mass  $891.66 \pm 0.26$  MeV and a narrow width  $50.8 \pm 0.9$  MeV [1]. Some recent experimental analyses [2–6] have precisely measured its resonance parameters. Moreover, a few theoretical efforts have been taken to calculate its hadronic coupling constant [7–9]. Since the  $K^*(892)$  meson is a low-lying vector meson with strangeness, a study of its decay width is definitely a straightforward investigation on the three-flavor structure of the low-energy hadronic interactions, hence, it is very helpful for us to acquaint with the dynamical traits of the hadronic interactions with QCD.

At present, lattice QCD is the most feasible approach from first principles to extract the resonance parameters of  $K^*(892)$  meson nonperturbatively. The principal decay channel (with a branching rate of 99.9%) of  $K^*(892)$  meson is to one pion plus one kaon in the  $p$ -wave [1], which can then be precisely dealt with on the lattice, and there is a pioneering lattice QCD study on its coupling constant  $g_{K^*\pi K}$  through evaluating appropriate three-point correlation function [10]. Among unstable hadrons, the vector  $\rho$  meson is ideal (see reasons in [11]) for lattice QCD investigations of a resonance, and it is extensively studied [10–18], nevertheless, so far, lattice QCD research on the resonance parameters of  $K^*(892)$  meson directly from  $p$ -wave scattering phase of  $\pi K$  system in the  $I = 1/2$  channel has not been reported yet, mainly because the rectangular diagram is exceptionally hard to rigorously calculate, the statistical error of the numeri-

cally computed  $K^*$  mass is not too small, and most of all, the proper finite size formula to describe  $\pi K$  system enclosed in a cubic box in the moving frame is not completely established yet until recently.

Motivated by the recent extensions and developments of the Rummukainen-Gottlieb formula [19] to a generic two-particle system with arbitrary masses in the moving frame [20–26] and J. Nebreda and J. Pelaez’s brilliant expositions on  $K^*(892)$  resonance [27], and also encouraged by our previous work on the accurate determination of  $K^*$  mass [28], the exploratory calculations of the scalar meson decay widths [21, 29, 30], and the accurate computation of the  $s$ -wave  $\pi K$  scattering length in the  $I = 1/2$  channel [31], here we will step out further to probe its decay width by way of lattice QCD.

In the present work, we discuss all the possible computation scheme for calculating the  $\pi K$  scattering phase with total zero momentum in the center-of-mass (CM) frame, and total non-zero momentum in the moving frame (MF), respectively, and obtain the  $K^*(892)$  decay width by calculating  $p$ -wave scattering phase of  $\pi K$  system in the  $I = 1/2$  channel in the moving frame. The calculations are launched on a MILC full QCD gauge configuration with the 2+1 flavors of the Asqtad improved staggered quarks [32, 33]. The meson masses quoted from our previous work [28] yielded  $(m_\pi + m_K)/m_{K^*} \approx 0.739$ , and the lattice ensemble parameters determined by the MILC collaboration gave the lattice extent  $L \approx 3.0$  fm and the lattice space inverse  $1/a = 1.373$  GeV [32, 33]. The Lüscher formula [34–36] is, as a usual, applied to the case in the center-of-mass frame, and we use a newly established finite size formula, which is the generalization of Rummukainen-Gottlieb formula [19] to the generic two-particle system in the moving frame [20–26], to estimate the  $p$ -wave  $\pi K$  scattering phase in the  $I = 1/2$  channel. The simulations conducted at two energies around the  $K^*$  resonance mass enable us to extract the decay width of the  $K^*(892)$  resonance.

\*Electronic address: fuziwen@scu.edu.cn

†Electronic address: gkanfu@gmail.com

This article is organized as follows. In Sec. II, we elaborate on our calculation method. Our concrete lattice calculations are provided in Sec. III. We deliver our results in Sec. IV, and reach our conclusions and outlooks in Sec. V. Numerical calculations of the zeta function are courteously supplied in the appendix for reference.

## II. FORMALISM AND METHOD OF MEASUREMENT

### A. The relativistic Breit-Wigner formula

The  $K^*(892)$  resonance possesses quantum numbers  $I(J^P) = \frac{1}{2}(1^-)$  and principally decays into one pion and one kaon in the  $p$ -wave with a branching rate of 99.9% [1]. For an elastic  $\pi K$  scattering in the resonance region, the relativistic Breit-Wigner formula (RBWF) for the  $p$ -wave scattering phase  $\delta_1$  can be written as [1]

$$\tan \delta_1 = \frac{\sqrt{s} \Gamma_R(s)}{M_R^2 - s}, \quad s = E_{CM}^2, \quad (1)$$

where  $M_R$  is the resonance position,  $\Gamma_R$  is decay width,  $E_{CM}$  is the center-of-mass energy, and  $s$  is the Mandelstam variable. The  $\Gamma_R(s)$  can be expressed by way of the effective  $K^* \rightarrow \pi K$  coupling constant  $g_{K^* \pi K}$  as [27],

$$\Gamma_R(s) = \frac{g_{K^* \pi K}^2 p^3}{6\pi s}, \quad (2)$$

$$p = \frac{1}{2\sqrt{s}} \sqrt{[s - (m_\pi - m_K)^2][s - (m_\pi + m_K)^2]},$$

Checking equations (1) and (2), a representation of the  $p$ -wave scattering phase as a function of the invariant mass  $\sqrt{s}$  is offered by the effective range formula (ERF),

$$\tan \delta_1 = \frac{g_{K^* \pi K}^2 p^3}{6\pi \sqrt{s}(M_R^2 - s)}, \quad (3)$$

which is applicable in the elastic region and suits the experimental measurements pretty well. The ERF permits us a fit or seeking for two unknown quantities: the coupling constant  $g_{K^* \pi K}$  and the resonance position  $M_R$  from the  $p$ -wave scattering phases. Then the  $K^*$  decay width is computed by

$$\Gamma_{K^*} = \Gamma_R(s) \Big|_{s=M_R^2} = \frac{g_{K^* \pi K}^2 p_{K^*}^3}{6\pi M_R^2}, \quad (4)$$

$$p_{K^*} = \frac{1}{2M_R} \sqrt{[M_R^2 - (m_\pi - m_K)^2][M_R^2 - (m_\pi + m_K)^2]}.$$

Equations (3) and (4) provide us an approach to derive the decay width  $\Gamma_{K^*}$  by studying the dependence of the  $p$ -wave  $\pi K$  scattering phase  $\delta_1$  on the invariant mass  $\sqrt{s}$ . We should stress at this point that we will extensively apply the ERF approximation in the present study since the RBWF holds perfectly for relatively narrower objects and the  $K^*(892)$  resonance has a pretty narrow decay width  $50.8 \pm 0.9$  MeV [1].

### B. Finite-volume methods

In this paper, we only focus on the  $\pi K$  system with the isospin representation of  $(I, I_z) = (1/2, 1/2)$  and deliberate on the  $K^*(892)$  meson decay into one pion plus one kaon in the  $p$ -wave.

#### 1. Center of mass frame

In the center-of-mass frame, the energy eigenvalues of the non-interacting  $\pi K$  system reads

$$E = \sqrt{m_\pi^2 + p^2} + \sqrt{m_K^2 + p^2},$$

where  $p = |\mathbf{p}|$ ,  $\mathbf{p} = (2\pi/L)\mathbf{n}$ , and  $\mathbf{n} \in \mathbb{Z}^3$ . The energies for the  $\mathbf{n} \neq 0$  are typically larger than the  $K^*$  resonance mass  $m_{K^*}$ . For example, the lowest energy for the  $\mathbf{n} \neq 0$  calculated from the previous determinations of  $m_\pi$ ,  $m_K$  and  $m_{K^*}$  [28] is  $E \approx 1.12 \times m_{K^*}$ , which is self-evidently not qualified to study the  $K^*(892)$  meson decay. Hence, we have no choice but to consider the  $\mathbf{n} = 0$  case, and the energy  $E = 0.739 \times m_{K^*}$ , which is still not a favorite option.

When considering the interaction between pion and kaon, the energy eigenstates of  $\pi K$  system are displaced by the hadronic interaction from  $E$  to  $\bar{E}$ , which are calculated by

$$\bar{E} = \sqrt{m_\pi^2 + k^2} + \sqrt{m_K^2 + k^2}, \quad k = \frac{2\pi}{L}q,$$

where the dimensionless momentum  $q \in \mathbb{R}$ . Solving this equation for the scattering momentum  $k$ , we have

$$k = \frac{1}{2\bar{E}} \sqrt{[\bar{E}^2 - (m_\pi - m_K)^2][\bar{E}^2 - (m_\pi + m_K)^2]}.$$

In this article, we are primarily interested in the energy eigenstates of  $\pi K$  system in the elastic region  $m_\pi + m_K < \bar{E} < 2(m_\pi + m_K)$ . In the center-of-mass frame these energy eigenstates transform as a vector (to be specific, the irreducible representation  $\Gamma = T_1^+$ ) under the cubic group  $O_h$ . The  $p$ -wave  $\pi K$  scattering phase  $\delta_1$  is linked to the energy  $\bar{E}$  by the Lüscher formula [34–36],

$$\tan \delta_1(k) = \frac{\pi^{3/2} q}{\mathcal{Z}_{00}(1; q^2)}, \quad (5)$$

where the zeta function is formally defined by

$$\mathcal{Z}_{00}(s; q^2) = \frac{1}{\sqrt{4\pi}} \sum_{\mathbf{n} \in \mathbb{Z}^3} \frac{1}{(|\mathbf{n}|^2 - q^2)^s}. \quad (6)$$

The  $\mathcal{Z}_{00}(s; q^2)$  has a finite value only when  $\text{Re } s > 3/2$ , nevertheless it could be analytically continued to  $s = 1$ . We usually evaluate  $\mathcal{Z}_{00}(s; q^2)$  using the way described in Ref. [37]. I notice that there exists an equivalent Lüscher formula in Ref. [38], which is the generalization of the Lüscher quantization condition to multiple two-body channels. Moreover it is easy to calculate and more accurate than Lüscher formula in the relativistic case.

## 2. Laboratory frame

To implement the physical kinematics such that the energy of  $\pi K$  system is pretty close to  $K^*$  meson mass, we recourse to the laboratory frame [19], which is usually called the moving frame. We have presented the detailed discussions of  $\pi K$  system in the moving frame in Ref. [30], here we just review its essential parts.

Considering a moving frame with non-zero total momentum  $\mathbf{P} = (2\pi/L)\mathbf{d}$ ,  $\mathbf{d} \in \mathbb{Z}^3$ , the energy eigenvalues of the free pion and kaon are

$$E_{MF} = \sqrt{m_\pi^2 + p_1^2} + \sqrt{m_K^2 + p_2^2},$$

where  $p_1 = |\mathbf{p}_1|$ ,  $p_2 = |\mathbf{p}_2|$ , and  $\mathbf{p}_1, \mathbf{p}_2$  define the three-momenta of  $\pi$  and  $K$ , respectively, which meet the periodic boundary condition (PBC),

$$\mathbf{p}_1 = \frac{2\pi}{L}\mathbf{n}_1, \quad \mathbf{p}_2 = \frac{2\pi}{L}\mathbf{n}_2, \quad \mathbf{n}_1, \mathbf{n}_2 \in \mathbb{Z}^3,$$

and total momentum  $\mathbf{P}$  satisfies  $\mathbf{P} = \mathbf{p}_1 + \mathbf{p}_2$ .

In the center of mass frame, the energy  $E_{CM}$  is

$$E_{CM} = \sqrt{m_\pi^2 + p^{*2}} + \sqrt{m_K^2 + p^{*2}},$$

where total center-of-mass momentum disappears, namely,  $p^* = |\mathbf{p}^*|$ ,  $\mathbf{p}^* = \mathbf{p}_1^* = -\mathbf{p}_2^*$ , here we denote the center-of-mass momenta with an asterisk (\*) [19]. We can readily verify that the  $\mathbf{p}^*$  are quantized to the values [30]

$$\mathbf{p}^* = \frac{2\pi}{L}\mathbf{r}, \quad \mathbf{r} \in P_{\mathbf{d}},$$

where the set  $P_{\mathbf{d}}$  is

$$P_{\mathbf{d}} = \left\{ \mathbf{r} \left| \mathbf{r} = \tilde{\gamma}^{-1} \left[ \mathbf{n} + \frac{\mathbf{d}}{2} \cdot \left( 1 + \frac{m_K^2 - m_\pi^2}{E_{CM}^2} \right) \right], \mathbf{n} \in \mathbb{Z}^3 \right. \right\}, \quad (7)$$

where the boost factor,  $\gamma = 1/\sqrt{1 - \mathbf{v}^2}$ , operates in the direction of the velocity  $\mathbf{v}$ , which is calculated from  $\mathbf{v} = \mathbf{P}/E_{MF}$ , and for the notational compactness we have taken the shorthand notation [19],

$$\tilde{\gamma}\mathbf{p} = \gamma\mathbf{p}_{\parallel} + \mathbf{p}_{\perp}, \quad \tilde{\gamma}^{-1}\mathbf{p} = \gamma^{-1}\mathbf{p}_{\parallel} + \mathbf{p}_{\perp}, \quad (8)$$

where  $\mathbf{p}_{\parallel}$  and  $\mathbf{p}_{\perp}$  are the ingredients of  $\mathbf{p}$  parallel and perpendicular to the center-of-mass velocity  $\mathbf{v}$ , respectively [19]:  $\mathbf{p}_{\parallel} = (\mathbf{p} \cdot \mathbf{v})\mathbf{v}/|\mathbf{v}|^2$ ,  $\mathbf{p}_{\perp} = \mathbf{p} - \mathbf{p}_{\parallel}$ .

Using the standard Lorentz transformation, the energy  $E_{CM}$  is connected to the  $E_{MF}$  through  $E_{CM} = \gamma^{-1}E_{MF}$ , or by  $E_{CM}^2 = E_{MF}^2 - \mathbf{P}^2$ .

We are particularly interested in one moving frame: pion at rest, kaon with the momentum  $\mathbf{p} = (2\pi/L)\mathbf{e}_3$  (namely,  $\mathbf{d} = \mathbf{e}_3$ ) and  $K^*(892)$  meson with the momentum  $\mathbf{P} = \mathbf{p}$ . For our concrete case, we found that its invariant mass takes  $\sqrt{s} = 0.8788 \times m_{K^*}$ , which is significantly closer to  $K^*$  meson mass  $m_{K^*}$  than that in the center-of-mass frame. Finally, we find one suitable to study  $K^*$  decay, and here we solely consider this case.

In the presence of the interaction between pion and kaon, the  $\overline{E}_{CM}$  can be calculated by

$$\overline{E}_{CM} = \sqrt{m_\pi^2 + k^2} + \sqrt{m_K^2 + k^2}, \quad k = \frac{2\pi}{L}q.$$

where the dimensional momentum  $q \in \mathbb{R}$ . Solving this equation for the scattering momentum  $k$ , we arrive at

$$k = \frac{1}{2\overline{E}} \sqrt{[\overline{E}_{CM}^2 - (m_\pi - m_K)^2][\overline{E}_{CM}^2 - (m_\pi + m_K)^2]}. \quad (9)$$

It is convenient to rewrite equation (9) to an elegant form for later use as

$$k^2 = \frac{1}{4} \left( \overline{E}_{CM} + \frac{m_\pi^2 - m_K^2}{\overline{E}_{CM}} \right)^2 - m_\pi^2, \quad (10)$$

which is used to calculate the scattering momentum  $k$  (including its statistical error), and investigate the lattice discretization effect.

The energy eigenstates of  $\pi K$  system for our moving frame transform under the tetragonal group  $C_{4v}$  [21]. Only the irreducible representations  $A_1$  and  $E$  are associated with the  $p$ -wave  $\pi K$  scattering states in a torus. We only compute the energies related with the  $A_1$  sector in the present study. The hadronic interaction displaces the energy eigenstate of  $\pi K$  system from  $E$  to  $\overline{E}$ , and the energy  $\overline{E}$  is linked to the  $p$ -wave  $\pi K$  scattering phase  $\delta_1$  with the help of newly established finite size formula in the moving frame for the generic two-particle system with arbitrary masses [20, 21, 23],

$$\tan \delta_1(k) = \frac{\gamma\pi^{3/2}q}{Z_{00}^{\mathbf{d}}(1; q^2) + \frac{2}{\sqrt{5}}q^{-2}Z_{20}^{\mathbf{d}}(1; q^2)}, \quad (11)$$

where we does not consider the higher scattering phase shifts  $\delta_l (l = 2, 3, 4, \dots)$  [22], and the modified zeta functions are formally defined by

$$\begin{aligned} Z_{00}^{\mathbf{d}}(s; q^2) &= \sum_{\mathbf{r} \in P_{\mathbf{d}}} \frac{1}{(|\mathbf{r}|^2 - q^2)^s}, \\ Z_{20}^{\mathbf{d}}(s; q^2) &= \sum_{\mathbf{r} \in P_{\mathbf{d}}} \frac{r^2 Y_{20}(\Omega_r)}{(r^2 - q^2)^s}, \end{aligned} \quad (12)$$

where  $\Omega_r$  represents the solid angle parameters  $(\theta, \phi)$  of  $\mathbf{r}$  in spherical coordinates and the  $Y_{lm}$  are the standard spherical harmonic functions, and the set  $P_{\mathbf{d}}$  is denoted in Eq. (7). The scattering momentum  $k$  is calculated from the invariant mass  $\sqrt{s}$  through  $\sqrt{s} = \sqrt{k^2 + m_\pi^2} + \sqrt{k^2 + m_K^2}$ . We have discussed the numerical calculation method of the  $Z_{00}^{\mathbf{d}}(1; q^2)$  in Appendix A of Ref. [30], and we will give the numerical calculation method of the  $Z_{20}^{\mathbf{d}}(1; q^2)$  in Appendix A although there are some general calculations of the zeta function  $Z_{lm}^{\mathbf{d}}(s; q^2)$  in Refs. [21, 22, 38].

### C. Correlation matrix

To compute two energy eigenvalues, i.e.,  $\bar{E}_n$  ( $n = 1, 2$ ), we constitute a  $2 \times 2$  correlation function matrix:

$$C(t) = \begin{pmatrix} \langle 0 | \mathcal{O}_{\pi K}^\dagger(t) \mathcal{O}_{\pi K}(0) | 0 \rangle & \langle 0 | \mathcal{O}_{\pi K}^\dagger(t) \mathcal{O}_{K^*}(0) | 0 \rangle \\ \langle 0 | \mathcal{O}_{K^*}^\dagger(t) \mathcal{O}_{\pi K}(0) | 0 \rangle & \langle 0 | \mathcal{O}_{K^*}^\dagger(t) \mathcal{O}_{K^*}(0) | 0 \rangle \end{pmatrix}, \quad (13)$$

where  $\mathcal{O}_{K^*}(t)$  is an interpolating operator for the vector  $K^*(892)$  meson with the specified momentum  $\mathbf{p} = (2\pi/L)\mathbf{e}_3$  and the polarization vector parallel to  $\mathbf{p}$ ;  $\mathcal{O}_{\pi K}(t)$  is an interpolating operator for the  $\pi K$  system with the given momentum  $\mathbf{p} = (2\pi/L)\mathbf{e}_3$ . These interpolating operators employed in the present work are actually identical to those in our previous studies [28, 31], nevertheless, to make this article self-contained, all the fundamental definitions will be provided in the following as well.

#### 1. $\pi K$ sector

Here we take advantage of the original definitions and notations [39–43] to examine the necessary formulae for the lattice QCD calculation of the  $p$ -wave scattering phase of  $\pi K$  system enclosed in a torus at the  $I = 1/2$  channel. Let us learn the elastic scattering of a Nambu-Goldstone pion with zero momentum and a Nambu-Goldstone kaon with the momentum  $\mathbf{p}$  in the Kogut-Susskind (KS) staggered fermion formalism. Using the interpolating operators  $\mathcal{O}_\pi(x_1), \mathcal{O}_\pi(x_3)$  for pions at points  $x_1, x_3$ , and  $\mathcal{O}_K(x_2), \mathcal{O}_K(x_4)$  for kaons at points  $x_2, x_4$ , respectively, the  $\pi K$  four-point functions are expressed as [43]

$$C_{\pi K}(x_4, x_3, x_2, x_1) = \langle \mathcal{O}_K(x_4) \mathcal{O}_\pi(x_3) \mathcal{O}_K^\dagger(x_2) \mathcal{O}_\pi^\dagger(x_1) \rangle.$$

where the pion and kaon interpolating field operators are denoted by [43]

$$\begin{aligned} \mathcal{O}_{\pi^+}(\mathbf{x}, t) &= -\bar{d}(\mathbf{x}, t) \gamma_5 u(\mathbf{x}, t), \\ \mathcal{O}_{\pi^0}(\mathbf{x}, t) &= \frac{1}{\sqrt{2}} [\bar{u}(\mathbf{x}, t) \gamma_5 u(\mathbf{x}, t) - \bar{d}(\mathbf{x}, t) \gamma_5 d(\mathbf{x}, t)], \\ \mathcal{O}_{K^0}(\mathbf{x}, t) &= \bar{s}(\mathbf{x}, t) \gamma_5 d(\mathbf{x}, t), \\ \mathcal{O}_{K^+}(\mathbf{x}, t) &= \bar{s}(\mathbf{x}, t) \gamma_5 u(\mathbf{x}, t). \end{aligned}$$

After carrying out the summation over the spatial coordinates  $\mathbf{x}_1, \mathbf{x}_2, \mathbf{x}_3$  and  $\mathbf{x}_4$ , we gain  $\pi K$  four-point function with the momentum  $\mathbf{p}$  as [30]

$$C_{\pi K}(\mathbf{p}; t_4, t_3, t_2, t_1) = \sum_{\mathbf{x}_1} \sum_{\mathbf{x}_2} \sum_{\mathbf{x}_3} \sum_{\mathbf{x}_4} e^{i\mathbf{p} \cdot (\mathbf{x}_4 - \mathbf{x}_2)} \times C_{\pi K}(x_4, x_3, x_2, x_1),$$

where  $x_1 \equiv (\mathbf{x}_1, t_1)$ ,  $x_2 \equiv (\mathbf{x}_2, t_2)$ ,  $x_3 \equiv (\mathbf{x}_3, t_3)$ , and  $x_4 \equiv (\mathbf{x}_4, t_4)$ . To refrain the color Fierz rearrangement of the quark lines [41], we choose  $t_1 \neq t_2 \neq t_3 \neq t_4$  and set  $t_1 = 0, t_2 = 1, t_3 = t$ , and  $t_4 = t + 1$ , respectively,

here  $t$  represents the time difference. We build the  $\pi K$  interpolating operator in the  $I = 1/2$  channel as [43]

$$\mathcal{O}_{\pi K}^{I=1/2}(\mathbf{p}, t) = \frac{1}{\sqrt{3}} \left\{ \sqrt{2} \pi^+(t) K^0(\mathbf{p}, t+1) - \pi^0(t) K^+(\mathbf{p}, t+1) \right\}, \quad (14)$$

where  $\mathbf{p}$  is total momentum of  $\pi K$  system. The  $\pi K$  operator has the isospin representation with  $(I, I_z) = (1/2, 1/2)$ .

Considering that  $u$  and  $d$  quarks have the equal mass, topologically only three quark line diagrams still contribute to  $\pi K$  scattering amplitudes [43]. These diagrams are elucidated in Fig. 1, and we usually label them as direct (D), crossed (C) and rectangular (R) diagrams, respectively [40, 41]<sup>1</sup>. The direct and crossed diagrams can be readily computed [40, 41] by means of only two fixed wall sources placed at the time slices  $t_1$  and  $t_2$ , which enables a relatively cheap lattice calculation of the  $I = 3/2$   $\pi K$  scattering length [44, 45]. Nevertheless, the rectangular diagram (R) needs extra quark propagator linking the time slices  $t_3$  and  $t_4$ , which make the strict evaluation of this diagram extraordinarily expensive.

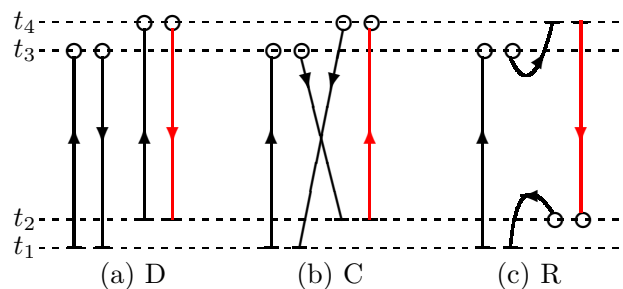


FIG. 1: (color online). Quark-link diagrams contributing to  $\pi K$  four-point functions. Short black bars stand for the wall sources. Open circles are sinks for local pion or kaon operators. The black lines represent for the  $u/d$  quark lines, and red lines stand for the strange quark lines.

Sasaki et al. handled this puzzle through the technique with a fixed kaon sink operator to save the computational resources [46]. Lang et al. recently solved this problem by the use of Laplacian-Heavyside smeared quarks within the distillation method [47]<sup>2</sup>. In our previous works [21, 30], we settled the question using the moving wall sources without gauge fixing introduced first by Kuramashi et al. [40, 41]. More specifically, we calculated these diagrams by computing each  $T$  quark propagators corresponding to the wall source at all the time

<sup>1</sup> In Ref. [43], they are denoted as  $A$ ,  $H$ , and  $X$ , respectively.

<sup>2</sup> It is well-known that the rectangular diagram (or backtracking contractions, box diagram [47]) is most challenging and important for the  $I = 1/2$  channel. And obtaining the reliable signal of it is vital to our final result. We observe that the signals of the rectangular diagram in Ref. [47] are at reasonable levels.

slice [21, 30, 40, 41],

$$\sum_{n''} D_{n', n''} G_t(n'') = \sum_{\mathbf{x}} \delta_{n', (\mathbf{x}, t)}, \quad 0 \leq t \leq T-1,$$

where  $D$  is the Dirac quark matrix, and the subscript  $t$  in the quark propagator  $G$  indicates the position of the wall source in the temporal direction [21, 30, 40, 41]. The associations of the quark propagators  $G_t(n)$  exploiting for

the  $\pi K$  four-point correlation functions are schematically illustrated in Fig. 1 [21, 30, 40, 41]. As we practiced in Ref. [30] for the study of  $\kappa$  decay width, for the non-zero momentum  $\mathbf{p}$ , we take an up quark source with 1, and a strange quark source with the  $e^{i\mathbf{p}\cdot\mathbf{x}}$  on each lattice site for the pion and kaon creation operator, respectively [30]. By means of the quark propagators  $G$ , we can represent  $D$ ,  $C$ , and  $R$  diagrams as [30]

$$\begin{aligned} C_{\pi K}^D(\mathbf{p}; t_4, t_3, t_2, t_1) &= \sum_{\mathbf{x}_3} \sum_{\mathbf{x}_4} e^{i\mathbf{p}\cdot\mathbf{x}_4} \langle \text{Tr}[G_{t_1}^\dagger(\mathbf{x}_3, t_3) G_{t_1}(\mathbf{x}_3, t_3)] \text{Tr}[G_{t_2}^\dagger(\mathbf{x}_4, t_4) G_{t_2}(\mathbf{x}_4, t_4)] \rangle, \\ C_{\pi K}^C(\mathbf{p}; t_4, t_3, t_2, t_1) &= \sum_{\mathbf{x}_3} \sum_{\mathbf{x}_4} e^{i\mathbf{p}\cdot\mathbf{x}_4} \langle \text{Tr}[G_{t_1}^\dagger(\mathbf{x}_3, t_3) G_{t_2}(\mathbf{x}_3, t_3) G_{t_2}^\dagger(\mathbf{x}_4, t_4) G_{t_1}(\mathbf{x}_4, t_4)] \rangle, \\ C_{\pi K}^R(\mathbf{p}; t_4, t_3, t_2, t_1) &= \sum_{\mathbf{x}_2} \sum_{\mathbf{x}_3} e^{i\mathbf{p}\cdot\mathbf{x}_2} \langle \text{Tr}[G_{t_1}^\dagger(\mathbf{x}_2, t_2) G_{t_4}(\mathbf{x}_2, t_2) G_{t_4}^\dagger(\mathbf{x}_3, t_3) G_{t_1}(\mathbf{x}_3, t_3)] \rangle, \end{aligned} \quad (15)$$

where the traces are taken over color, and the hermiticity natures of the quark propagator  $G$  have been applied to remove the  $\gamma^5$  factors [21, 30, 40, 41].

As discussed in Refs. [40, 41], the rectangular diagram  $R$  produce the gauge-variant noise, and we usually reduce it by conducting the gauge field average without gauge fixing as we practiced in Refs. [21, 30, 48, 49]. All the three quark line diagrams in Fig. 1 are needed to compute the  $p$ -wave  $\pi K$  scattering phase in the  $I = 1/2$  channel. In the isospin limit, the  $\pi K$  four-point function in the  $I = 1/2$  channel can be described in terms of only three quark line diagrams [43],

$$\begin{aligned} C_{\pi K}(\mathbf{p}, t) &\equiv \langle \mathcal{O}_{\pi K}(\mathbf{p}, t) | \mathcal{O}_{\pi K}(\mathbf{0}, 0) \rangle \\ &= D + \frac{1}{2} N_f C - \frac{3}{2} N_f R, \end{aligned} \quad (16)$$

where the interpolating field operator  $\mathcal{O}_{\pi K}$  denoted in Eq. (14) generates a  $\pi K$  state with the total isospin 1/2 and momentum  $\mathbf{p}$ , and  $N_f$  is the staggered-flavor factor, which is plugged in to address for the flavor degrees of freedom of the KS staggered fermion [39]. We should bear firmly in mind that if we carry out the appropriate root of the staggered fermion determinant<sup>3</sup>, in the continuum limit, the same number of the flavors flow around the internal quark loops as in QCD [39]. Therefore, at the level of these quark line diagrams (namely,  $D$ ,  $C$ , and  $R$ ), all contributions are exactly as in QCD [39].

In practice, we compute the ratios as well<sup>4</sup>

$$R^X(t) = \frac{C_{\pi K}^X(\mathbf{p}; 0, 1, t, t+1)}{C_\pi(\mathbf{0}; 0, t) C_K(\mathbf{p}; 1, t+1)}, \quad X = D, C, \text{ and } R, \quad (17)$$

where  $C_\pi(\mathbf{0}; 0, t)$  and  $C_K(\mathbf{p}; 1, t+1)$  are the  $\pi$  and  $K$  correlators with the momentum  $\mathbf{0}$  and  $\mathbf{p}$ , respectively.

We should bear in memory that the dedications of non-Nambu-Goldstone pion and kaon in the intermediate states are exponentially reduced for the large time owing to their heavier masses compared with these of Nambu-Goldstone pion and kaon [21, 30, 39–41]. Thus, we can ignore this systematic error due to other  $\pi K$  tastes.

## 2. $K^*(892)$ sector

In principle, we can calculate the propagators for two local vector  $K^*$  meson,  $\gamma_i \otimes \gamma_i$  (VT) and  $\gamma_0 \gamma_i \otimes \gamma_0 \gamma_i$  (PV)[60, 61]. However, here we simply quote the results for local VT  $K^*$  meson since it delivers quite stable results in the analysis of the mass spectrum. Moreover, the numerical evaluation of  $K^* \rightarrow \pi K$  three-point function is much eased if we adopt local VT  $K^*$  operator. Thus, we use an interpolation operator with the isospin  $I = 1/2$  and  $J^P = 1^-$  at the source and sink [28], namely,

$$\mathcal{O}(x) \equiv \sum_a u_a(x) \gamma_i \otimes \gamma_i \bar{s}_a(x),$$

<sup>3</sup> There are some strong evidences to demonstrate that the contribution from a single Dirac fermion can be nicely restored by carrying out the fourth root of the fermion determinant, see more details in Ref [50]. In the present work, we suppose that the fourth-root procedure reproduces the proper continuum limit of QCD, and the lattice results of this work rely on this hypothesis. Please consult Refs. [51–59] for the recent investigations about the fourth-root recipe.

<sup>4</sup> If imposing the Dirichlet boundary condition in the temporal direction, we can easily extract the energy shift  $\delta E$  from ratios  $R^X$  [40, 41]. On the other hand, we can readily check that when  $t \ll T/2$ , even we set the PBC in the temporal direction, we still can roughly estimate  $\delta E$  from these ratios.

where  $a$  is the color index. The time slice correlator for the  $K^*$  meson in the momentum  $\mathbf{p}$  state is computed by

$$C_{K^*}(\mathbf{p}, t) = \sum_{\mathbf{x}} \sum_{a,b} e^{i\mathbf{p}\cdot\mathbf{x}} \langle u_b(\mathbf{x}, t) \gamma_i \otimes \gamma_i \bar{s}_b(\mathbf{x}, t) \times s_a(\mathbf{0}, 0) \gamma_i \otimes \gamma_i \bar{u}_g^a(\mathbf{0}, 0) \rangle,$$

where  $\mathbf{0}, \mathbf{x}$  are the spatial points of the  $K^*$  state at source and sink, respectively.

For the staggered quarks, the meson correlators have the general single-particle representation,

$$\mathcal{C}(t) = \sum_i A_i e^{-m_i t} + \sum_i A'_i (-1)^t e^{-m'_i t} + (t \rightarrow N_t - t),$$

where the oscillating terms correspond to a meson with the opposite parity. For  $K^*$  meson correlator, we take only one mass with each parity, and the oscillating parity partner is the  $p$ -wave meson with the  $J^P = 1^+$ . The  $K_1$  meson is with  $J^P = 1^+$ , so it is the candidate of the oscillating parity partner of the vector  $K^*$  meson. However, these states with  $J^P = 1^+$  can just as well be multihadron states<sup>5</sup>. With staggered fermions, the multihadron possibilities include the various taste combinations. So we can not identify its parity partner with the  $K_1$ , see more discussions in Ref. [28]. Thus, the  $K^*(892)$  correlator was fit to

$$C_{K^*}(t) = b_{K^*} e^{-m_{K^*} t} + b_{K_1} (-1)^t e^{-M_{K_1} t} + (t \rightarrow N_t - t), \quad (18)$$

where  $b_{K_1}$  and  $b_{K^*}$  are two overlap factors.

### 3. Off-diagonal sector

A calculation of the generic three-point function are briefly discussed in Ref. [10]. To rigorously evaluate it we must compute a spatial volume number of propagators, namely  $N_L^3$  ( $16^3$  for our case). To avoid the apparent intractability of the exactly computing this problem, S. Goltlieb et al. introduced the ‘‘exponential’’ method, which calculate a two-point function with the presence of a source, and then differentiates with the source strength to achieve the corresponding three-point functions [7, 8]. To investigate vector meson decay into pseudoscalars from quenched lattice QCD [10], Loft and DeGrand adopted ‘‘two-stage’’ technique [62, 63], which takes approximately twice as compared with the calculation of the mass spectra [10]. Later, when studying the resonance parameter of the vector  $\rho$  meson [10–18], people chiefly employ a stochastic method [64–66] or its variants to evaluate three-point correlation function.

Motivated by the precisely evaluate the  $\pi\pi$  four-point correlation functions by Kuramashi et al [40, 41] with the moving wall source technique [31], analogously, we have

successfully extended this technique to evaluate three-point correlation function, and obtained pretty good signals for the three-point functions of the  $\pi\pi \rightarrow \sigma$  [29] and  $\pi K \rightarrow \kappa$  [30]. In this work we will continue to use this technique to evaluate the  $\pi K \rightarrow K^*$  three-point correlation function.

To prevent the tangled color Fierz transformation of the quark lines [41], we should choose  $t_1 \neq t_2 \neq t_3$ . In practice, we pick  $t_1 = 0, t_2 = 1$ , and  $t_3 = t$  for the  $\pi K \rightarrow K^*$  three-point correlation function, and opt  $t_1 = 0, t_2 = t$ , and  $t_3 = t + 1$  for the  $K^* \rightarrow \pi K$  three-point correlation function. The quark line diagrams corresponding to the  $K^* \rightarrow \pi K$  and  $\pi K \rightarrow K^*$  three-point functions are schematically illustrated in Fig. 2(a) and Fig. 2(b), respectively.

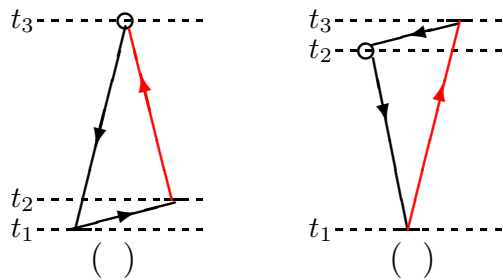


FIG. 2: (color online). Quark-link diagrams contributing to  $\pi K \rightarrow K^*$  and  $K^* \rightarrow \pi K$  three-point correlation functions. Short black bars stand for the wall sources. The black lines represent for the  $u/d$  quark lines, and the red lines stand for the strange quark lines. (a) Quark contractions of  $\pi K \rightarrow K^*$ , where open circle is the sink for local  $K^*$  operator. (b) Quark contractions of  $K^* \rightarrow \pi K$ , where open circle is the sink for local pion operator.

The  $\pi K \rightarrow K^*$  three-point function can be easily evaluated with only two fixed wall sources [21, 30]. Nevertheless, the computation of  $K^* \rightarrow \pi K$  three-point function is pretty hard, since it requires the extra quark propagator linking time slices  $t_2$  and  $t_3$  [21, 30]. In practice, we employ an up quark source with 1 on each site for pion creation operator, and a strange quark source with  $e^{i\mathbf{p}\cdot\mathbf{x}}$  on each lattice site for kaon creation operator [30]. We write the  $K^* \rightarrow \pi K$  and  $\pi K \rightarrow K^*$  three-point functions in terms of the quark propagators  $G$ ,

$$C_{\pi K \rightarrow K^*}(\mathbf{p}; t_3, t_2, t_1) = \sum_{\mathbf{x}_3, \mathbf{x}_2} e^{i\mathbf{p}\cdot\mathbf{x}_3} \langle \text{Tr}[G_{t_2}(\mathbf{x}_3, t_3) \gamma_5 \times G_{t_1}^\dagger(\mathbf{x}_3, t_3) \gamma_3 G_{t_1}(\mathbf{x}_2, t_2)] \gamma_5 \rangle, \\ C_{K^* \rightarrow \pi K}(\mathbf{p}; t_3, t_2, t_1) = \sum_{\mathbf{x}_2, \mathbf{x}_3} e^{i\mathbf{p}\cdot\mathbf{x}_2} \langle \text{Tr}[G_{t_3}(\mathbf{x}_2, t_2) \gamma_3 \times G_{t_1}^\dagger(\mathbf{x}_2, t_2) \gamma_5 G_{t_1}(\mathbf{x}_3, t_3)] \gamma_5 \rangle, \quad (19)$$

where trace is over the color index; the Dirac matrix are used as an interpolating field for the  $i$ th meson:  $\gamma_5$  for pseudoscalars and  $\gamma_3$  for the vector meson.

<sup>5</sup> Private communication, C. DeTar (2012).

## D. Extraction of energies

To map out “avoided level crossings” between the  $K^*$  resonance and its decay products, it is important to use the variational method [36] to separate the ground state from the first excited state by calculating a  $2 \times 2$  correlation function matrix  $C(t)$  denoted in (13). For this purpose, we construct a ratio of the correlation function matrices as

$$M(t, t_R) = C(t) C^{-1}(t_R), \quad (20)$$

with some reference time  $t_R$  [36] to extract two lowest energy eigenvalues  $\bar{E}_n$  ( $n = 1, 2$ ), which can be obtained by a cosh-fit to two eigenvalues  $\lambda_n(t, t_R)$  ( $n = 1, 2$ ) of the correlation matrix  $M(t, t_R)$ . Considering the use of the staggered fermion, it is easy to verify that  $\lambda_n(t, t_R)$  ( $n = 1, 2$ ) explicitly has an oscillating term [67–69],

$$\lambda_n(t, t_R) = A_n \cosh \left[ -E_n \left( t - \frac{T}{2} \right) \right] + (-1)^t B_n \cosh \left[ -E'_n \left( t - \frac{T}{2} \right) \right], \quad (21)$$

for a large  $t$ , which mean  $0 \ll t_R < t \ll T/2$  to suppress both the excited states and wrap-around contributions [30, 70–72]<sup>6</sup>. Without loss of generality, we suppose  $\lambda_1(t, t_R) > \lambda_2(t, t_R)$ .

## III. LATTICE CALCULATION

### A. Simulation parameters

We use the MILC full QCD gauge configurations in the presence of the  $N_f = 2 + 1$  flavors of the Asqtad-improved staggered fermions [60, 61] and a Symanzik-improved gluon action [73]. We should keep in memory that the MILC gauge configurations are generated using the staggered formulation of lattice fermions [74] with the fourth root of the fermion determinant [60].

We measured the  $\pi K$  four-point correlation functions on the 0.15 fm MILC “medium” coarse lattice ensemble of  $400 \times 20^3 \times 48$  gauge configurations with the bare quark masses  $am_{ud} = 0.00484$  and  $am_s = 0.0484$  and bare gauge coupling  $10/g^2 = 6.566$ . The inverse lattice spacing  $a^{-1} = 1.373_{-14}^{+34}$  GeV and the lattice extent  $L \approx 3.0$  fm [32, 33]. The mass of the dynamical strange quark is quite close to its physical value, and the masses of the  $u$  and  $d$  quarks are degenerate [32, 33]. The more detailed descriptions of the simulation parameters can be found in Refs. [32, 33]. The PBC is imposed to three spatial directions and temporal direction.

## B. Computations

We employ the standard conjugate gradient method to achieve the necessary matrix element of the inverse Dirac fermion matrix to compute the  $\pi K$  four-point functions. We compute the correlators on all the time slices, and explicitly combine the results from each of the  $N_T = 48$  time slices. To be specific, the diagonal correlator  $C_{11}(t)$  is measured through

$$\begin{aligned} C_{11}(t) &= \left\langle (\pi K)(t) (\pi K)^\dagger(0) \right\rangle \\ &= \frac{1}{T} \sum_{t_s} \left\langle (\pi K)(t + t_s) (\pi K)^\dagger(t_s) \right\rangle. \end{aligned}$$

After averaging the propagator over all  $N_T = 48$  possible values, we found that the statistics are significantly improved.

For each time slice, six Dirac fermion matrix inversions are needed to compute for the possible 3 color choices for the pion source and kaon source, respectively. So, totally we carry out 288 matrix inversions on a single gauge configuration. This big number of the matrix inversions, conducted on 400 MILC gauge configurations, furnishes the gigantic statistics required to precisely compute the  $\pi K$  four-point correlation functions.

For the another diagonal correlator  $C_{22}(t)$ ,  $K^*(892)$  correlator, we simply exploit the available propagators measured in our previous study [28] to calculate the  $K^*(892)$  correlator

$$C_{22}(t) = \frac{1}{T} \sum_{t_s} \left\langle K^{*\dagger}(t + t_s) K^*(t_s) \right\rangle,$$

where we sum the correlator over all the time slices and average it too.

We evaluate the first off-diagonal correlator  $C_{21}(t)$ : the  $\pi K \rightarrow K^*$  three-point function, through

$$\begin{aligned} C_{21}(t) &= \left\langle K^*(t) (\pi K)^\dagger(0) \right\rangle \\ &= \frac{1}{T} \sum_{t_s} \left\langle K^*(t + t_s) (\pi K)^\dagger(t_s) \right\rangle, \end{aligned}$$

where the summation is over all the time slice. Through the relation  $C_{12}(t) = C_{21}^*(t)$ , we can gratuitously gain the second off-diagonal correlator  $C_{12}(t)$ : the  $K^* \rightarrow \pi K$  three-point function.

In the present study, we evaluate two-point correlation functions for pion and kaon as well,

$$\begin{aligned} G_\pi(\mathbf{0}; t) &= \frac{1}{T} \sum_{t_s} \langle 0 | \pi^\dagger(\mathbf{0}, t + t_s) \pi(\mathbf{0}, t_s) | 0 \rangle, \\ G_K(\mathbf{p}; t) &= \frac{1}{T} \sum_{t_s} \langle 0 | K^\dagger(\mathbf{p}, t + t_s) K(\mathbf{p}, t_s) | 0 \rangle, \quad (22) \end{aligned}$$

where the summation is over all the time slice, and the  $G_\pi(\mathbf{0}; t)$ ,  $G_K(\mathbf{p}; t)$  are the two-point correlation functions for pion meson with zero momentum, and kaon meson with the momentum  $\mathbf{p}$ , respectively.

<sup>6</sup> In Ref. [30], we gave a detailed discussion about a contamination from “wraparound” effects. In practice, we will select the fitting time ranges satisfying  $t_{\max} \leq 16$ , and reasonably neglect it.

#### IV. SIMULATION RESULTS

In our previous work [28], we have measured the point-to-point pion and kaon correlators with high accuracy. Exploiting these correlators, we can precisely derive the pion mass ( $m_\pi$ ) and kaon mass ( $m_K$ ), which are in fair agreement with the previous MILC determinations in Ref. [33]. In Table I we list the pion mass  $m_\pi$ , the mass  $m_K$  and energy  $E_K$  of kaon meson with the momentum  $\mathbf{p} = (2\pi/L)\mathbf{e}_3$ , which are extracted through a single exponential fit ansatz to  $G_\pi(t; \mathbf{0})$  and  $G_K(t; \mathbf{p})$  in Eq. (22). We show the mass  $m_{K^*}$  and energy  $E_{K^*}$  of the vector  $K^*$  meson with the momentum  $\mathbf{p} = (2\pi/L)\mathbf{e}_3$  as well, which are extracted from the  $K^*(892)$  correlator.

TABLE I: Masses  $m$  of the pion, kaon and  $K^*(892)$  mesons, and energies  $E$  of kaon and  $K^*(892)$  mesons with the momentum  $\mathbf{p} = (2\pi/L)\mathbf{e}_3$ , extracted from the corresponding point-to-point correlation functions.

	$\pi$	K	$K^*(892)$
$am$	0.17503(17)	0.39913(27)	0.7757(70)
$aE$		0.50465(48)	0.8278(82)

We must stress at this point that, in the present work, we just use this calculated  $K^*(892)$  mass  $m_{K^*}$  to indicate the position of free  $K^*(892)$  mass, which are marked by the fancy cyan plus point in Fig. 7, and we visualize this value to compare with the resonance mass  $M_R$ .

##### A. Diagrams D, C, and R

The individual ratios  $R^X$  ( $X = D, C$  and  $R$ ), which correspond to the diagrams in Fig. 1, are illustrated in Fig. 3 as the functions of time separation  $t$ . The values of the direct amplitude ratio  $R^D$  are pretty close to unity, implying a quite slight interaction in this channel. On the other hand, the crossed amplitude ratio  $R^C$  increases linearly, hinting a repulsive force in this channel. Moreover, after a starting increase up to  $t \sim 4$ , the rectangular amplitude ratio  $R^R$  demonstrates a roughly linear decrease up until  $t \sim 15$ , and the signals become noisy after that, suggesting an attractive force between pion and kaon in this channel. These characteristics are what we expected from the theoretical predictions [39, 75].

We can observe that the crossed and rectangular amplitudes take the same value at  $t = 0$ , and the similar values for small  $t$ . Since our analytical representations for both amplitudes are identical at this value of  $t$ , they should manifest analogously until the asymptotic  $\pi K$  state is reached. Clear signals observed up to  $t = 15$  for the rectangular amplitude demonstrate that the technique of the moving wall source without gauge fixing used here is practical and feasible.

According to the analytical arguments in Ref. [76], we can readily infer that the ratio for the rectangular di-

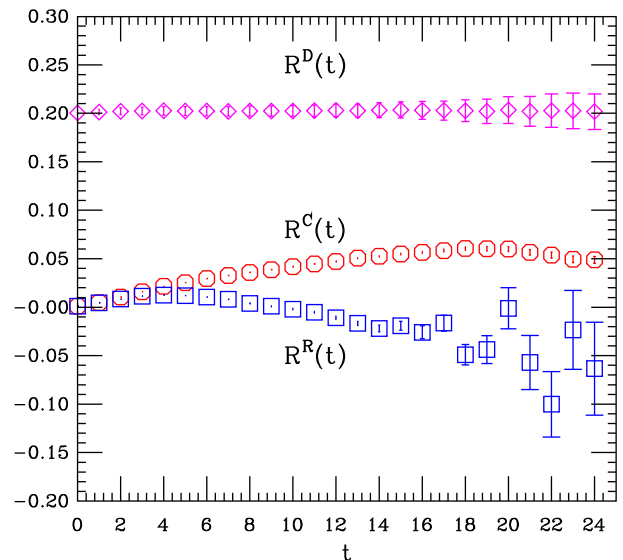


FIG. 3: (color online). Individual amplitude ratios  $R^X(t)$  ( $X = D, C$  and  $R$ ) for the  $\pi K$  four-point correlation function measured by the moving wall source without gauge fixing as the functions of  $t$ . Direct diagram (magenta diamonds) shifted by 0.8, crossed diagram (red octagons) and rectangular diagrams (blue squares).

agram  $R^R$  has errors, which should increase exponentially as  $e^{m_K t}$  for large time separation. The magnitude of the errors is in quantitative agreement with this theoretical prediction as displayed in Fig. 4. Fitting the errors  $\delta R^R(t)$  by a single exponential fit ansatz  $\delta R^R(t) \sim \exp(\mu_R t)$  over the range  $10 \leq t \leq 16$ , we can achieve the corresponding fitting values of  $\mu_R$  with  $a\mu_R = 0.358$ , which can be reasonably compared with the corresponding kaon masses  $m_K$  determined in our previous work [28], which is also listed in Table I. This demonstrates, on the other side, that the technique of the moving wall source without gauge fixing used in this work is practically feasible.

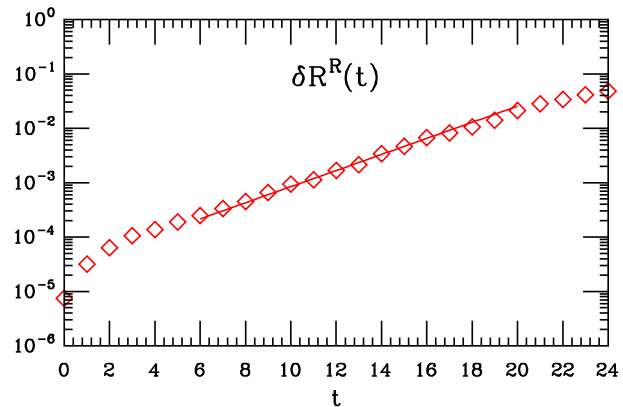


FIG. 4: (color online). The error of ratio  $R^R(t)$  as a function of time separation  $t$ . Solid line is a single exponential fit over the range  $10 \leq t \leq 16$ .



## B. Energy eigenvalues

We calculate two eigenvalues  $\lambda_n(t, t_R)$  ( $n = 1, 2$ ) for the matrix  $M(t, t_R)$  denoted in Eq. (20) with the reference time  $t_R = 5$ . In Fig. 5 we illustrate our lattice simulation results for  $\lambda_n(t, t_R)$  ( $n = 1, 2$ ) in a logarithmic scale as a function of time separation  $t$  along with a correlated fit to the asymptotic form offered in Eq. (21). From these fits the desired energies  $\overline{E}_n$  ( $n = 1, 2$ ) are then obtained, and which will be employed to derive the  $p$ -wave scattering phase.

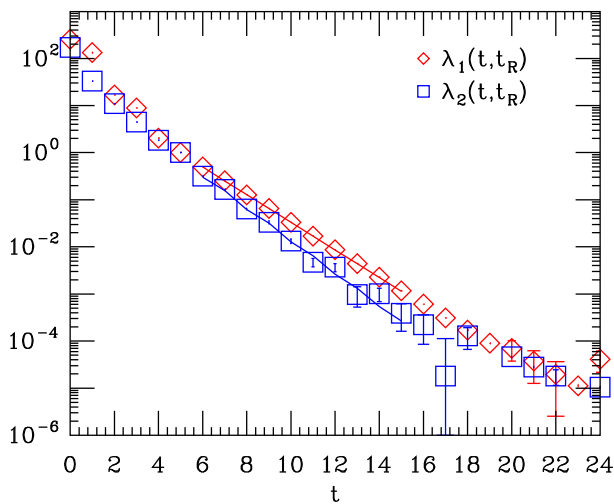


FIG. 5: (color online). The eigenvalues  $\lambda_1(t, t_R)$  and  $\lambda_2(t, t_R)$  as a function of  $t$ . Occasional points with negative central values for the eigenvalue  $\lambda_2(t, t_R)$  are not plotted. The solid lines are the correlated fits to the asymptotic form denoted in Eq. (21), from which the energy eigenvalues  $\overline{E}_n$  ( $n = 1, 2$ ) are extracted. The lower curve ( $n = 2$ ) is slightly steeper than the upper curve ( $n = 1$ ).

As we noticed in Refs. [29–31], we realize that the properly extracting the energy eigenvalues is vital to our final conclusions. Since the PBC is imposed on three spatial directions and the temporal direction, we should suppress the warp-around contaminations [11, 31]. By defining a fitting range  $[t_{\min}, t_{\max}]$  and varying the values of the minimum fitting distance  $t_{\min}$  and the maximum fitting distance  $t_{\max}$ , we obtain these energies in a correct manner. In practice, we make  $t_{\min} = t_R + 1$  and increase reference time  $t_R$  to reduce excited contaminations [11]. At the same time, we opt  $t_{\max}$  to be away from the time slice  $T/2$  to reduce the warp-around effects [11]. Furthermore, we extract two eigenvalues  $\lambda_n$  ( $n = 1, 2$ ) with the “effective energy” plots [11, 31], a variant of the effective mass plots, and they were fit to Eq. (21) by changing  $t_{\min}$ , and with the  $t_{\max}$  either at 15 or where the fractional statistical errors exceeded about 20% for two successive time slices. The effective energy plots as a function of  $t_{\min}$  are illustrated in Fig. 6.

The energy eigenvalues  $\overline{E}_n$  ( $n = 1, 2$ ) were chosen by looking for the combination of a “plateau” in the effective

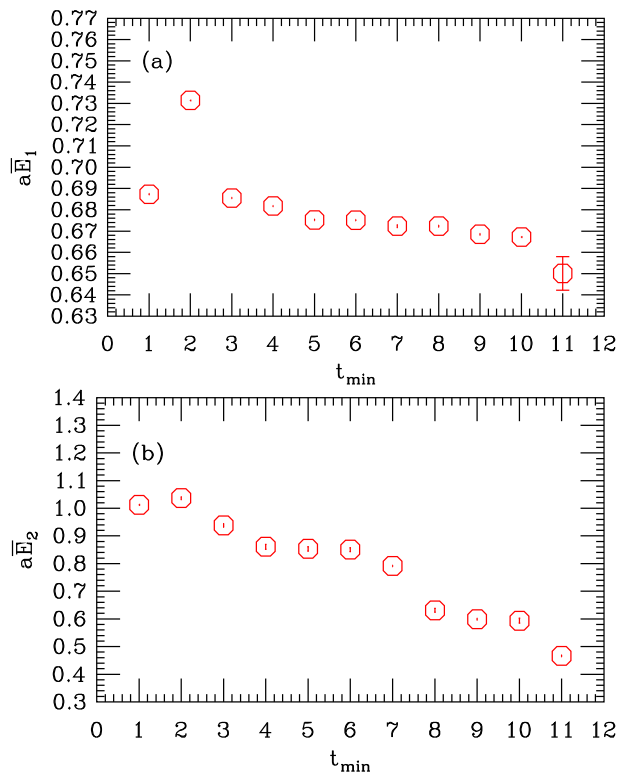


FIG. 6: The effective energy plots,  $a\overline{E}_n$  ( $n = 1, 2$ ), as the functions of  $t_{\min}$ . (a) The effective energy plot for  $\overline{E}_1$  and (b) that for  $\overline{E}_2$

energy plots as the function of  $t_{\min}$  and a reasonable fit quality [11, 31]. We observed that the effective energies take only relatively small errors within a minimum time distance region  $5 \leq t_{\min} \leq 8$  for  $\overline{E}_1$  and  $5 \leq t_{\min} \leq 6$  for  $\overline{E}_2$ , respectively. The fitted numbers for  $\overline{E}_n$  ( $n = 1, 2$ ) along with the fitting parameters  $t_R$ ,  $t_{\min}$  and  $t_{\max}$ , fit quality  $\chi^2/\text{dof}$  are summarized in Table II.

TABLE II: The fitted values of the energy eigenvalues for the ground state ( $n = 1$ ) and the first excited state ( $n = 2$ ). Here we tabulate the reference time  $t_R$ , the fitting range,  $t_{\min}$  and  $t_{\max}$ , the number of degrees of freedom (dof) for the fit quality  $\chi^2/\text{dof}$  and the fitted results for the energy eigenvalues  $\overline{E}_n$  ( $n = 1, 2$ ) in lattice units.

$n$	$t_R$	$t_{\min}$	$t_{\max}$	$a\overline{E}_n$	$\chi^2/\text{dof}$
1	5	6	15	0.67507(40)	12.2/6
2	5	6	15	0.8534(78)	9.6/6

The energy of the pion and kaon in non-interacting case (namely,  $E_1$ ) is computed from the pion mass  $m_\pi$  and kaon energy  $E_K$  listed in Table I as  $E_1 = m_\pi + E_K$ . This number is listed in Table III. We distinctly observe that  $\overline{E}_1 < E_1 < \overline{E}_2$ , which mean that the  $p$ -wave scattering phase for  $\lambda_1(t, t_R)$  and  $\lambda_2(t, t_R)$  is positive and negative, respectively. This evidently reveals that there exist a resonance between  $\overline{E}_1$  and  $\overline{E}_2$ .

TABLE III: Summary of the energy eigenvalues  $\overline{E}_n$  ( $n = 1, 2$ ) and  $p$ -wave scattering phase  $\delta_1$  for  $\pi K$  system in a cubic box.  $E_1$  is the energy of the free pion-kaon system.  $\overline{E}_n$  ( $n = 1, 2$ ) are obtained from the correlated fits to eigenvalues  $\lambda_n(t, t_R)$  ( $n = 1, 2$ ). The invariant mass  $\sqrt{s}$ , the scattering momentum  $k$  and the  $p$ -wave scattering phase  $\delta_1$  derived through the expression (23) in the continuum are regarded as *Cont*, and those achieved with the equation (24) on the lattice are viewed as *Lat*. The scattering momentum  $k_0$  is computed by  $k_0^2 = 1/4 \times (\sqrt{s} + (m_\pi^2 - m_K^2)/\sqrt{s})^2 - m_\pi^2$ . All values with the mass dimension are in lattice units.

	$n = 1$		$n = 2$	
$E_n$	0.67968(51)		—	
$\overline{E}_n$	0.67507(40)		0.8534(78)	
	Cont	Lat	Cont	Lat
$\sqrt{s}$	0.59751(45)	0.60350(45)	0.7934(84)	0.8004(84)
$k^2$	0.00588(13)	0.00750(14)	0.0690(30)	0.0729(31)
$k_0^2$	—	0.00745(13)	—	0.0717(30)
$\tan \delta_1$	0.0294(93)	0.0091(22)	-2.01(43)	-2.48(63)
$\sin^2 \delta_1$	0.00087(55)	0.000083(39)	0.802(68)	0.860(62)

### C. Finite-size effects

We should pay attention to the discretisation error (or truncation error) inherent in the special finite size formula for  $\pi K$  system denoted in (11) [21, 30]. It stems from the Lorentz transformation from the moving frame to the center-of-mass frame. When applying the Lorentz symmetry in the continuum limit, we utilize the following relations [21, 30],

$$\begin{aligned} \sqrt{s} &= \sqrt{E_{MF}^2 - p^2}, \\ k^2 &= \frac{1}{4} \left( \sqrt{s} + \frac{m_\pi^2 - m_K^2}{\sqrt{s}} \right)^2 - m_\pi^2, \end{aligned} \quad (23)$$

in the Lorentz transformation for the invariant mass  $\sqrt{s}$ , the energy of the  $\pi K$  system in the moving frame  $E_{MF}$  and the scattering momentum  $k$ . Nevertheless, the discretisation effects definitely violate the Lorentz symmetry on the lattice and equation (23) is only effective up to the truncation errors.

Following the recommendations in Ref. [30], we calculate the invariant mass  $\sqrt{s}$  and the scattering momentum  $k$  from the energy in the moving frame  $E_{MF}$  of  $\pi K$  system using

$$\begin{aligned} \cosh(\sqrt{s}) &= \cosh(E_{MF}) - 2 \sin^2 \left( \frac{p}{2} \right), \\ 2 \sin^2(k/2) &= \cosh \left( \frac{\sqrt{s}}{2} + \frac{m_\pi^2 - m_K^2}{2\sqrt{s}} \right) - \cosh(m_\pi), \end{aligned} \quad (24)$$

and derive the  $p$ -wave scattering phase  $\delta_1$  by inserting the scattering momentum  $k$  into the finite-size formula in Eq. (11). We have justified these formula in Ref. [30], and we will employ them in this work to investigate the discretisation effects.

To grasp these discretisation effects quantitatively, in the present study we compute the invariant mass  $\sqrt{s}$  and the scattering momentum  $k$  not only from the energy momentum relation in the continuum (23) but also from that on the lattice (24), and subsequently extract the  $p$ -wave scattering phase  $\delta_1$ . People usually regard the disparity stemming from two options of the energy momentum relations as the discretisation error. Since it is a kind of truncation error, it is expected to smaller if we employ the lattice ensemble with smaller lattice space  $a$ , of course it should be disappeared in the continuum limit. The results for the  $p$ -wave scattering phase  $\delta_1$  along with the invariant mass  $\sqrt{s}$  and the scattering momentum  $k$  are summarized in Table III.

### D. Extraction of the scattering phase and decay width

The noticeable differences in the invariant mass  $\sqrt{s}$  and scattering momentum  $k$  because of the discretisation effects are obviously observed from Table III. Moreover, the differences for the  $p$ -wave scattering phase  $\delta_1$  due to the discretization effects are impressive, and can be comparable with the statistical errors, even considerably larger than its statistical error for the  $n = 1$  case. These characteristics are visualized in Fig. 7, where the  $p$ -wave scattering phase  $\sin^2 \delta_1$  is displayed instead [16, 30]. We notice, from Table III, that the numerical value of the  $p$ -wave scattering phase  $\delta_1$  at the invariant mass  $\sqrt{s} < m_{K^*}$  ( $am_{K^*} = 0.7757 \pm 0.0070$ ) is positive due to an attractive interaction, and that at  $\sqrt{s} > m_{K^*}$  is negative owing to a repulsive interaction. These features indicate a resonance at a mass around the  $K^*$  mass.

In principle, it is a piece of cake to extract the  $K^*$  meson decay width through fitting the  $p$ -wave scattering phase shift data with the effective range formula directly [16, 30]. Nevertheless, in this work we studied with the quark mass which is larger than its nature value and the kinematic factor in the decay width depends clearly upon the quark mass [27], thus an extrapolation is indispensable [16, 30]. However, we carried out a lattice calculation with one set of the quark mass in this exploratory investigation, therefore, we have no choice but to adopt an alternative method [16, 30]. As we explained in section II A, the resonant characteristic of the  $p$ -wave scattering phase  $\delta_1$  are parameterized with the coupling constant  $g_{K^*\pi K}$ ,

$$\tan \delta_1 = \frac{g_{K^*\pi K}^2}{6\pi} \frac{k^3}{\sqrt{s}(M_R^2 - s)}, \quad (25)$$

where  $M_R$  is the resonance mass.

According to the elaborations in Refs. [27, 77], we can fairly suppose that the coupling constant  $g_{K^*\pi K}$  changes quite slowly and smoothly with the quark mass. Therefore, the equation (25) enables us to solve for two unknown quantities, that is, the coupling constant  $g_{K^*\pi K}$ , and the resonance mass  $M_R$  [16, 30].

According to the discussions in Refs. [16, 30], in practice, we usually employ the scattering momentum  $k_0$  instead of  $k$  when applying Eq. (25). In Table III, we provide the scattering momentum  $k_0$  calculated by  $k_0^2 = 1/4 \times (\sqrt{s} + (m_\pi^2 - m_{K^*}^2)/\sqrt{s})^2 - m_\pi^2$  in addition to  $k$ . We can observe that the difference between  $k$  and  $k_0$  is not significant, and we can neglect this systemic error for the present study [16, 30].

When we utilize the energy-momentum relations (23) in the continuum, the lattice simulation results of the coupling constant  $g_{K^*\pi K}$  and the resonance mass  $M_R$  solved by Eq. (25) are

$$\begin{aligned} g_{K^*\pi K} &= 11.73 \pm 2.08, \\ M_R &= 0.739(20), \\ M_R/m_{K^*} &= 0.953(28), \end{aligned} \quad (26)$$

where the  $K^*$  meson mass  $m_{K^*}$  is quoted from our previous work [28].

On the other hand, if we adopt the energy momentum relations (24) on the lattice, we gain the simulation results as

$$\begin{aligned} g_{K^*\pi K} &= 6.38(78), \\ M_R &= 0.7873(97), \\ M_R/m_{K^*} &= 1.015(16). \end{aligned} \quad (27)$$

This obtained value of the coupling constant  $g_{K^*\pi K}$  in lattice case is in fair agreement with  $g_{K^*\pi K} \approx 5.5$ , which are obtained by Nebreda and Peláez from the residue of the amplitude at the pole position in Ref. [27]. Moreover, it is in reasonable agreement with the experimental observable  $g_{K^*\pi K} = 5.64(35)$  evaluated from the PDG estimations of the decay width  $\Gamma_{K^*} = 50.8(9)$  MeV [1] within the statistical error.

In Fig. 7, we illustrate the curves for  $\sin^2 \delta_1$  achieved by equation (25) with the coupling constant  $g_{K^*\pi K}$  and the resonance mass  $M_R$  provided in Eq. (26) and Eq. (27), respectively. The positions of the resonance mass  $M_R$ , are courteously marked in Fig. 7 for the two cases (black cross and red plus for the continuum and lattice cases, respectively). For visualized comparisons, we mark the  $K^*(892)$  mass  $m_{K^*}$  with fancy cyan plus as well. We can observe that the resonance mass  $M_R$  for lattice case is in reasonable accordance with the  $K^*(892)$  mass  $m_{K^*}$ .

Supposing that the dependence of the coupling constant  $g_{K^*\pi K}$  on the quark mass is ignorable [27, 77], we can roughly estimate the  $K^*(892)$  meson decay width at the physical quark mass as

$$\Gamma^{\text{phy}} = \frac{g_{K^*\pi K}^2 (k^{\text{phy}})^3}{6\pi (m_{K^*}^{\text{phy}})^2}, \quad (28)$$

where  $m_{K^*}^{\text{phy}} = 891.66(26)$  MeV is the physical  $K^*(892)$  meson mass, which we take from the current PDG [1], and the scattering momentum  $k^{\text{phy}}$  at the physical point is calculated by

$$(k^{\text{phy}})^2 = \frac{1}{4} \left( m_{K^*}^{\text{phy}} + \frac{(m_\pi^{\text{phy}})^2 - (m_{K^*}^{\text{phy}})^2}{m_{K^*}^{\text{phy}}} \right)^2 - (m_\pi^{\text{phy}})^2,$$

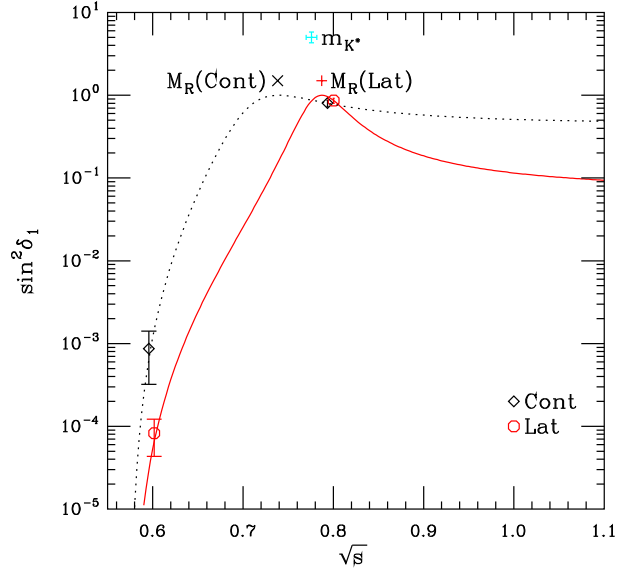


FIG. 7: (color online). The scattering phase  $\sin^2 \delta_1$  and the positions of the  $K^*$  meson mass  $m_{K^*}$  and resonance mass  $M_R$ . The simulation results achieved with the energy-momentum expressions in the continuum (23) are viewed as **Cont** and those with the relations on the lattice (24) as **Lat**. The two lines are achieved by Eq. (25) with the quantities  $g_{K^*\pi K}$  and  $M_R$  provided in Eq. (26) and Eq. (27), respectively. The abscissa is in lattice units.

where  $m_\pi^{\text{phy}}$  is physical pion mass ( $m_\pi^{\text{phy}} = 139.57018(35)$  MeV) and  $m_{K^*}^{\text{phy}}$  is physical kaon mass ( $m_{K^*}^{\text{phy}} = 493.677(13)$  MeV) which are quoted from the PDG [1]. This produces

$$\Gamma^{\text{phy}} = (219 \pm 39) \text{ MeV} \quad (29)$$

where we utilize the simulation result given in Eq. (26). On the other hand, if we use these given in Eq. (27), it yields

$$\Gamma^{\text{phy}} = (64.9 \pm 8.0) \text{ MeV}. \quad (30)$$

The estimation in lattice case given in Eq. (30) is in fair agreement with the corresponding PDG quantity for the  $K^* \rightarrow \pi K$  decay width, namely,  $\Gamma_{K^*} = 50.8 \pm 0.9$  MeV. We can observe that the difference stemming from our two options of the energy-momentum relations is much larger than the statistical error, which indicate that the proper correction of the discretization errors is absolutely necessary.

These results are quite stimulating, considering that we make a big assumption that the coupling constant  $g_{K^*\pi K}$  is independent upon the quark mass, and we carry out an extrapolation, etc. Anyway, one thing greatly comforts us is that we use the pion mass (about 240 MeV) which is pretty close to its realistic value (about 140 MeV), so we don't carry out a long extrapolation.

## V. CONCLUSIONS AND OUTLOOKS

In the present work, we have carried out a lattice QCD computation of the  $p$ -wave  $\pi K$  scattering phase in the  $I = 1/2$  channel near the  $K^*(892)$  resonance region in the moving frame with total non-zero momentum for the MILC “medium” coarse ( $a \approx 0.15$  fm) lattice ensemble with the  $N_f = 2 + 1$  flavors of the Asqtad improved staggered fermions. We employed the technique with the moving wall source without gauge fixing [31] introduced by Kuramashi et al. in Refs. [40, 41] to calculate all the three diagrams classified in Ref. [43] with high precision. We have exhibited that the lattice QCD computation of the  $p$ -wave scattering phase for the  $I = 1/2$   $\pi K$  system and then the estimation of the decay width of  $K^*(892)$  meson are feasible even with our present limited computing resources. The scattering phase data clearly reveals a resonance at a mass around the  $K^*(892)$  meson mass obtained in our previous study [28]. Most of all, we extracted the  $K^*(892)$  meson decay width from the scattering phase data and demonstrated that it is reasonably comparable with the  $K^*(892)$  meson decay width quoted from PDG within the statistical error.

We have adopted the effective range formula, which allows us to exploit the effective  $K^* \rightarrow \pi K$  coupling constant  $g_{K^*\pi K}$  to extrapolate from our lattice simulation point  $(m_\pi + m_K)/m_{K^*} = 0.7388$  to the physical point  $(m_\pi + m_K)/m_{K^*} = 0.7102$ , assuming that the coupling constant  $g_{K^*\pi K}$  is independent of the quark mass. This is a crude estimation, a more rigorous computation of the decay width is highly desirable. As we pointed out above, the decay width can be reliably estimated from the energy dependence of the scattering phase data by fitting the BWRf if we carry out the lattice simulations close to the physical quark mass and obtain several energies near the resonance mass. We will keep on enthusiastically requesting for the possible computational allocations to fulfil this valuable work.

Nevertheless, we should bear firmly in mind that some critical issues should be resolved in the more convincing calculation. One is to reduce the discretization errors, which, we illustrated in the previous section, are significantly larger than the corresponding statistical errors. A naïve way to handle this question is to utilize a lattice ensemble closer to the continuum limit. Another challenging and stimulating topic is to suppress the contaminations of the  $p$ -wave scattering phase from the  $d$ -wave scattering phase or higher, which we preliminarily touched on this topic for the  $\pi K$  system in Ref. [21], see more valuable discussions in Ref. [22]. Moreover, the comprehensive investigations on the lattice size dependence of the scattering phase is absolutely fascinating. Nevertheless, all of these open questions are beyond the scope of this paper since this will demand a huge amount of computing allocations. We postpone these expensive tasks in our future study.

This work concentrated on the  $p$ -wave scattering phase only at two energies for a single lattice ensemble. Since

we had only a small number of energies at hand, it becomes quite difficult to reliably map out the resonance region. Therefore, our current lattice results are not comparable with the experimentally measured quantities. Although a reliable derivation of the  $K^*(892)$  resonance parameters from the lattice is absolutely big challenging and most prospective, our rudimentary work reported here can be still viewed as an important conceptual study, and the techniques employed here will be helpful and useful for other resonances such as the  $D^*$ , possibly even for some exotic hadrons.

### Acknowledgments

We deeply appreciate the MILC Collaboration for supplying us the Asqtad lattice ensemble and MILC codes. We should thank NERSC (National Energy Research Scientific Center) for providing the convenient platform to download the MILC gauge configurations and Massimo Di Pierro for his Python toolkits. The authors sincerely thank Carleton DeTar for his encouraging and critical comments and supplying us the fitting software. We especially thank Eulogio Oset for his enlightening and constructive comments and corrections. We are grateful to Hou Qing for his supports. Numerical calculations for this paper were carried out at AMAX, CENTOS and HP workstations in the Institute of Nuclear Science and Technology, Sichuan University.

### Appendix A: The numerical evaluation of the $\mathcal{Z}_{20}^{\mathbf{d}}(1; q^2)$ function

In this appendix we follow the original derivations and notations in Refs. [22, 30, 37] to provide one simple approach for the numerical evaluation of the zeta function  $\mathcal{Z}_{20}^{\mathbf{d}}(s; q^2)$  defined in Eq. (12) in the moving frame for the arbitrary value of  $q^2$ .

The definition of the zeta function  $\mathcal{Z}_{20}^{\mathbf{d}}(s; q^2)$  appeared in Eq. (12) is

$$\mathcal{Z}_{20}^{\mathbf{d}}(s; q^2) = \sum_{\mathbf{r} \in P_{\mathbf{d}}} \frac{\mathcal{Y}_{20}(\mathbf{r})}{(r^2 - q^2)^s}, \quad (\text{A1})$$

where  $\mathcal{Y}_{lm}(\mathbf{r}) \equiv r^l Y_{lm}(\Omega_r)$ .  $\Omega_r$  represents the solid angles  $(\theta, \phi)$  of  $\mathbf{r}$  in spherical coordinates and the  $Y_{lm}$  are the spherical harmonic functions, and the summation for  $\mathbf{r}$  is taken over the set

$$P_{\mathbf{d}} = \left\{ \mathbf{r} \mid \mathbf{r} = \bar{\gamma}^{-1} \left( \mathbf{n} + \frac{\alpha}{2} \mathbf{d} \right), \quad \mathbf{n} \in \mathbb{Z}^3 \right\}, \quad (\text{A2})$$

where

$$\alpha = 1 + \frac{m_K^2 - m_\pi^2}{E_{CM}^2},$$

and the operation  $\hat{\gamma}^{-1}$  is defined in Eq. (8).

Without loss of generality, we first assume  $q^2 > 0$ , and divide the summation in  $\mathcal{Z}_{20}$  into two pieces as

$$\sum_{\mathbf{r} \in P_{\mathbf{d}}} \frac{\mathcal{Y}_{20}(\mathbf{r})}{(r^2 - q^2)^s} = \sum_{r^2 < q^2} \frac{\mathcal{Y}_{20}(\mathbf{r})}{(r^2 - q^2)^s} + \sum_{r^2 > q^2} \frac{\mathcal{Y}_{20}(\mathbf{r})}{(r^2 - q^2)^s}, \quad (\text{A3})$$

$$\begin{aligned} \sum_{r^2 > q^2} \frac{\mathcal{Y}_{20}(\mathbf{r})}{(r^2 - q^2)^s} &= \frac{1}{\Gamma(s)} \sum_{r^2 > q^2} \mathcal{Y}_{20}(\mathbf{r}) \left[ \int_0^1 dt t^{s-1} e^{-t(r^2 - q^2)} + \int_1^\infty dt t^{s-1} e^{-t(r^2 - q^2)} \right] \\ &= \frac{1}{\Gamma(s)} \int_0^1 dt t^{s-1} e^{q^2 t} \sum_{\mathbf{r} \in P_{\mathbf{d}}} \mathcal{Y}_{20}(\mathbf{r}) e^{-r^2 t} - \sum_{r^2 < q^2} \frac{\mathcal{Y}_{20}(\mathbf{r})}{(r^2 - q^2)^s} + \sum_{\mathbf{r} \in P_{\mathbf{d}}} \mathcal{Y}_{20}(\mathbf{r}) \frac{e^{-(r^2 - q^2)}}{(r^2 - q^2)^s}. \end{aligned} \quad (\text{A4})$$

The second term nicely counteract the first term in Eq. (A3). Using the Poisson resummation formula, the first term results in

$$\begin{aligned} \text{first term} &= \frac{1}{\Gamma(s)} \int_0^1 dt t^{s-1} e^{tq^2} \sum_{\mathbf{n} \in \mathbb{Z}^3} f_{\mathbf{n}}, \\ f_{\mathbf{n}} &\equiv \int d^3 \mathbf{x} \mathcal{Y}_{20}(\mathbf{r}) e^{-t|\mathbf{r}|^2 + i2\pi \mathbf{n} \cdot \mathbf{x}}, \end{aligned} \quad (\text{A5})$$

where  $\mathbf{r} = \hat{\gamma}^{-1}(\mathbf{x} + \frac{1}{2}\alpha \mathbf{d})$ . After transforming the integration variable from  $\mathbf{x}$  to  $\mathbf{r}$ , and considering the relations:  $d^3 \mathbf{x} = \gamma d^3 \mathbf{r}$  and  $\mathbf{x} = \hat{\gamma} \mathbf{r} - \frac{1}{2}\alpha \mathbf{d}$ , then we can separate terms which are dependent only upon  $\mathbf{r}$

$$f_{\mathbf{n}} \equiv \gamma e^{-i\pi \alpha \mathbf{n} \cdot \mathbf{d}} \int d^3 \mathbf{r} \mathcal{Y}_{20}(\mathbf{r}) e^{-t|\mathbf{r}|^2 + i2\pi \hat{\gamma} \mathbf{n} \cdot \mathbf{r}}.$$

Let  $\mathbf{k} \equiv \pi \hat{\gamma} \mathbf{n}$ , we rewrite above equation as

$$f_{\mathbf{n}} \equiv \gamma e^{-i\pi \alpha \mathbf{n} \cdot \mathbf{d}} e^{-k^2/t^2} \int d^3 \mathbf{r} \mathcal{Y}_{20}(\mathbf{r}) e^{-t(\mathbf{r} - i\mathbf{k}/t)^2},$$

where  $\mathbf{r} = (x, y, z)$ . Let us conduct a variable substitution, namely,  $\mathbf{r} - i\mathbf{k}/t \rightarrow \mathbf{r}$ , we can strictly verify

$$\begin{aligned} \int d^3 \mathbf{r} x^2 e^{-t(\mathbf{r} - i\mathbf{k}/t)^2} &= \frac{2\pi}{t} \int_0^\infty dx \left( x^2 - \frac{k_x^2}{t^2} \right) e^{-tx^2} \\ &= \left( \frac{\pi}{t} \right)^{3/2} \left( \frac{1}{2t} - \frac{k_x^2}{t^2} \right), \\ \int d^3 \mathbf{r} y^2 e^{-t(\mathbf{r} - i\mathbf{k}/t)^2} &= \left( \frac{\pi}{t} \right)^{3/2} \left( \frac{1}{2t} - \frac{k_y^2}{t^2} \right), \\ \int d^3 \mathbf{r} z^2 e^{-t(\mathbf{r} - i\mathbf{k}/t)^2} &= \left( \frac{\pi}{t} \right)^{3/2} \left( \frac{1}{2t} - \frac{k_z^2}{t^2} \right). \end{aligned} \quad (\text{A6})$$

We finally obtain

$$f_{\mathbf{n}} \equiv -\gamma e^{-i\pi \alpha \mathbf{n} \cdot \mathbf{d}} e^{-k^2/t^2} \frac{\pi^{3/2}}{t^{7/2}} \mathcal{Y}_{20}(\mathbf{k}),$$

where  $\mathcal{Y}_{20}(\mathbf{k}) \equiv k^2 Y_{20}(\Omega_k)$ . Now we can rewrite the first term in Eq. (A4) as

$$\text{first term} = \frac{\gamma}{\Gamma(s)} \int_0^1 dt t^{s-1} e^{tq^2} \frac{\pi^{3/2}}{t^{7/2}} \sum_{\mathbf{n} \in \mathbb{Z}^3} (\pi \hat{\gamma} \mathbf{n})^2 Y_{20}(\Omega_k)$$

where the summation over  $\mathbf{r}$  is conducted with  $\mathbf{r} \in P_{\mathbf{d}}$  denoted in Eq. (A2). The second term can be conveniently delivered in an integral expression,

$$\times e^{i\pi \alpha \mathbf{n} \cdot \mathbf{d}} e^{-(i\pi \hat{\gamma} \mathbf{n})^2/t}. \quad (\text{A7})$$

After collecting all terms, it leads to the representation of the zeta function at  $s = 1$ ,

$$\begin{aligned} \mathcal{Z}_{20}^{\mathbf{d}}(1; q^2) &= \sum_{\mathbf{r} \in P_{\mathbf{d}}} r^2 Y_{20}(\Omega_r) \frac{e^{-(r^2 - q^2)}}{r^2 - q^2} \\ &\quad - \int_0^1 dt e^{tq^2} \frac{\pi^{3/2}}{t^{7/2}} \sum_{\mathbf{n} \in \mathbb{Z}^3} (\pi \hat{\gamma} \mathbf{n})^2 Y_{20}(\Omega_k) \\ &\quad \times e^{-i\pi \alpha \mathbf{n} \cdot \mathbf{d}} e^{-(\pi \hat{\gamma} \mathbf{n})^2/t}. \end{aligned} \quad (\text{A8})$$

Now let us consider the case of  $q^2 \leq 0$ . As a matter of fact, there is no need for us to divide the summation in  $\mathcal{Z}_{20}^{\mathbf{d}}(s; q^2)$  into two parts, and can be delivered in an integral expression as well [30, 31]. Conducting the same procedures, we obtain the same expression in Eq. (A8). Therefore, equation (A8) is applicable for the arbitrary value of  $q^2$ .

Plugging in  $\mathbf{d} = (0, 0, 1)$  into equation (A8), we arrive at the representation of the zeta function  $\mathcal{Z}_{20}^{\mathbf{d}}(s; q^2)$  in Eq. (12) devoted for the current work

$$\begin{aligned} \mathcal{Z}_{20}^{\mathbf{d}}(1; q^2) &= \sum_{\mathbf{r} \in P_{\mathbf{d}}} r^2 Y_{20}(\Omega_r) \frac{e^{-(r^2 - q^2)}}{r^2 - q^2} \\ &\quad - \int_0^1 dt e^{tq^2} \frac{\pi^{3/2}}{t^{7/2}} \sum_{\mathbf{n} \in \mathbb{Z}^3} (\pi \hat{\gamma} \mathbf{n})^2 Y_{20}(\Omega_k) \\ &\quad \times \cos(\pi \alpha \mathbf{n} \cdot \mathbf{d}) e^{-(\pi \hat{\gamma} \mathbf{n})^2/t}, \end{aligned} \quad (\text{A9})$$

where only the real part of the zeta function  $\mathcal{Z}_{20}^{\mathbf{d}}(1; q^2)$  is survived.

I also note that the general numerical evaluation of the zeta function  $\mathcal{Z}_{lm}^{\mathbf{d}}(s; q^2)$  has been derived in Refs. [21, 22]. We numerically compared both these representations of the zeta function  $\mathcal{Z}_{20}(1; q^2)$  with this representation, and found that they are reasonable consistent.

- 
- [1] J. Beringer *et al.* [Particle Data Group Collaboration], Phys. Rev. D **86**, 010001 (2012).
- [2] M. Ablikim *et al.* [BES Collaboration], Phys. Lett. B **633**, 681 (2006) [hep-ex/0506055].
- [3] J. Z. Bai *et al.* [BES Collaboration], [hep-ex/0304001].
- [4] D. R. Boito, R. Escribano and M. Jamin, JHEP **1009**, 031 (2010) [arXiv:1007.1858 [hep-ph]].
- [5] R. E. Mitchell *et al.* [CLEO Collaboration], Phys. Rev. D **79**, 072008 (2009) [arXiv:0903.1301 [hep-ex]].
- [6] B. Aubert *et al.* [BABAR Collaboration], Phys. Rev. D **76**, 012008 (2007) [arXiv:0704.0630 [hep-ex]].
- [7] S. A. Gottlieb, P. B. MacKenzie, H. B. Thacker and D. Weingarten, Nucl. Phys. B **263**, 704 (1986).
- [8] S. A. Gottlieb, P. B. Mackenzie, H. B. Thacker and D. Weingarten, Phys. Lett. B **134**, 346 (1984).
- [9] N. Vasanti, Nucl. Phys. B **118**, 533 (1977).
- [10] R. D. Loft and T. A. DeGrand, Phys. Rev. D **39**, 2692 (1989).
- [11] X. Feng, K. Jansen, D. B. Renner, Phys. Rev. D **83**, 094505 (2011) [arXiv:1011.5288 [hep-lat]].
- [12] R. L. Altmeyer, M. Gockeler, R. Horsley, E. Laermann, G. Schierholz and P. M. Zerwas, Z. Phys. C **68**, 443 (1995) [hep-lat/9504003].
- [13] C. McNeile *et al.* [UKQCD Collaboration], Phys. Lett. B **556**, 177 (2003) [hep-lat/0212020].
- [14] S. Aoki *et al.* [CP-PACS Collaboration], Phys. Rev. D **76**, 094506 (2007) [arXiv:0708.3705 [hep-lat]].
- [15] N. Ishizuka [PACS-CS Collaboration], PoS LATTICE **2011**, 125 (2011) [arXiv:1111.0377 [hep-lat]].
- [16] S. Aoki *et al.* [CS Collaboration], Phys. Rev. D **84**, 094505 (2011) [arXiv:1106.5365 [hep-lat]].
- [17] C. B. Lang, D. Mohler, S. Prelovsek and M. Vidmar, Phys. Rev. D **84**, 054503 (2011) [arXiv:1105.5636 [hep-lat]].
- [18] J. Frison *et al.* PoS LATTICE **2010** (2010) 139 [arXiv:1011.3413 [hep-lat]].
- [19] K. Rummukainen, S. A. Gottlieb, Nucl. Phys. B **450**, 397 (1995) [arXiv:hep-lat/9503028 [hep-lat]].
- [20] Z. Davoudi and M. J. Savage, Phys. Rev. D **84** (2011) 114502 [arXiv:1108.5371 [hep-lat]].
- [21] Z. Fu, Phys. Rev. D **85**, 014506 (2012) [arXiv:1110.0319 [hep-lat]].
- [22] L. Leskovec and S. Prelovsek, Phys. Rev. D **85**, 114507 (2012) [arXiv:1202.2145 [hep-lat]].
- [23] M. Gockeler, R. Horsley, M. Lage, U. -G. Meissner, P. E. L. Rakow, A. Rusetsky, G. Schierholz and J. M. Zanotti, arXiv:1206.4141 [hep-lat].
- [24] M. Doring, U. G. Meissner, E. Oset and A. Rusetsky, Eur. Phys. J. A **48**, 114 (2012) [arXiv:1205.4838 [hep-lat]].
- [25] M. T. Hansen and S. R. Sharpe, arXiv:1204.0826 [hep-lat].
- [26] V. Bernard, D. Hoja, U. G. Meissner and A. Rusetsky, arXiv:1205.4642 [hep-lat].
- [27] J. Nebreda, J. R. Peláez., Phys. Rev. D **81**, 054035 (2010) [arXiv:1001.5237 [hep-ph]].
- [28] Ziwen Fu and Kan Fu, *Lattice QCD study on  $I = 1/2$  low-lying mesons*, in preparation.
- [29] Z. Fu, JHEP **1207**, 142 (2012) [arXiv:1202.5834 [hep-lat]].
- [30] Z. Fu, JHEP **1201**, 017 (2012) [arXiv:1110.5975 [hep-lat]].
- [31] Z. Fu, Phys. Rev. D **85**, 074501 (2012) [arXiv:1110.1422 [hep-lat]].
- [32] C. Bernard *et al.*, Phys. Rev. D **83**, 034503 (2011) [arXiv:1003.1937 [hep-lat]].
- [33] A. Bazavov, D. Toussaint, C. Bernard, J. Laiho, C. DeTar, L. Levkova, M. B. Oktay, S. Gottlieb *et al.*, Rev. Mod. Phys. **82**, 1349 (2010) [arXiv:0903.3598 [hep-lat]].
- [34] M. Lüscher, Nucl. Phys. B **354**, 531 (1991).
- [35] L. Lellouch, M. Luscher, Commun. Math. Phys. **219**, 31 (2001) [hep-lat/0003023].
- [36] M. Luscher, U. Wolff, Nucl. Phys. B **339**, 222 (1990).
- [37] T. Yamazaki *et al.* [CP-PACS Collaboration], Phys. Rev. D **70**, 074513 (2004) [hep-lat/0402025].
- [38] M. Doring, U. -G. Meissner, E. Oset and A. Rusetsky, Eur. Phys. J. A **47**, 139 (2011) [arXiv:1107.3988 [hep-lat]].
- [39] S. R. Sharpe, R. Gupta, G. W. Kilcup, Nucl. Phys. B **383**, 309 (1992).
- [40] Y. Kuramashi, M. Fukugita, H. Mino, M. Okawa, A. Ukawa, Phys. Rev. Lett. **71**, 2387 (1993).
- [41] M. Fukugita, Y. Kuramashi, M. Okawa, H. Mino, A. Ukawa, Phys. Rev. D **52**, 3003 (1995) [hep-lat/9501024].
- [42] M. Fukugita, Y. Kuramashi, H. Mino, M. Okawa, A. Ukawa, Phys. Rev. Lett. **73**, 2176 (1994) [hep-lat/9407012].
- [43] J. Nagata, S. Muroya, A. Nakamura, Phys. Rev. C **80**, 045203 (2009) [arXiv:0812.1753 [hep-lat]].
- [44] C. Miao, X. Du, G. Meng, C. Liu, Phys. Lett. B **595**, 400 (2004).
- [45] S. R. Beane, P. F. Bedaque, T. C. Luu, K. Orginos, E. Pallante, A. Parreno and M. J. Savage, Phys. Rev. D **74**, 114503 (2006).
- [46] K. Sasaki *et al.* [PACS-CS Collaboration], Prog. Theor. Phys. Suppl. **186**, 187 (2010).
- [47] C. B. Lang, L. Leskovec, D. Mohler and S. Prelovsek, *K pi scattering for isospin 1/2 and 3/2 in lattice QCD*, arXiv:1207.3204
- [48] Z. Fu, arXiv:1201.3708 [hep-lat].
- [49] Z. Fu, Commun. Theor. Phys. **57**, 78 (2012) [arXiv:1110.3918 [hep-lat]].
- [50] *Lattice Methods for Quantum Chromodynamics*, by Thomas DeGrand and Carleton DeTar, World Scientific, ISBN 981-256-727-5 (2006).
- [51] S. Dürr, C. Hoelbling and U. Wenger, Phys. Rev. D **70**, 094502 (2004).
- [52] C. Bernard, Phys. Rev. D **73**, 114503 (2006) [arXiv:hep-lat/0603011].
- [53] C. Bernard, M. Golterman, Y. Shamir and S. R. Sharpe, Phys. Lett. B **649**, 235 (2007) [arXiv:hep-lat/0603027].
- [54] M. Creutz, Phys. Lett. B **649**, 241 (2007).
- [55] C. Bernard, M. Golterman and Y. Shamir, Phys. Rev. D **73**, 114511 (2006) [arXiv:hep-lat/0604017].
- [56] M. Creutz, Phys. Lett. B **649**, 230 (2007) [arXiv:hep-lat/0701018].
- [57] S. Dürr and C. Hoelbling, Phys. Rev. D **71**, 054501 (2005) [arXiv:hep-lat/0411022].
- [58] S. Dürr and C. Hoelbling, Phys. Rev. D **74**, 014513 (2006) [arXiv:hep-lat/0604005].
- [59] A. Hasenfratz and R. Hoffmann, Phys. Rev. D **74**, 014511

- (2006) [arXiv:hep-lat/0604010].
- [60] C. W. Bernard *et al.*, Phys. Rev. D **64**, 054506 (2001) [arXiv:hep-lat/0104002].
- [61] C. Aubin *et al.*, Phys. Rev. D **70**, 094505 (2004) [arXiv:hep-lat/0402030].
- [62] C. W. Bernard, T. Draper, G. Hockney and A. Soni, In Wuppertal 1985, Proceedings, Lattice Gauge Theory\*, 199-207
- [63] C. W. Bernard, T. Draper, G. Hockney, A. M. Rushton and A. Soni, Phys. Rev. Lett. **55**, 2770 (1985).
- [64] I. T. Drummond, S. Duane and R. R. Horgan, Nucl. Phys. B **220**, 119 (1983).
- [65] S. -J. Dong and K. -F. Liu, Phys. Lett. B **328**, 130 (1994) [hep-lat/9308015].
- [66] M. Foster *et al.* [UKQCD Collaboration], Phys. Rev. D **59**, 074503 (1999) [hep-lat/9810021].
- [67] D. Barkai, K. J. M. Moriarty and C. Rebbi, Phys. Lett. B **156**, 385 (1985).
- [68] A. Mihály, H. R. Fiebig, H. Markum and K. Rabitsch, Phys. Rev. D **55**, 3077 (1997).
- [69] A. Mihály, Ph.D. thesis, Lajos Kossuth University, Debrecen, 1998.
- [70] R. Gupta, A. Patel and S. R. Sharpe, Phys. Rev. D **48**, 388 (1993).
- [71] X. Feng, K. Jansen and D. B. Renner, Phys. Lett. B **684** 268 (2010) [arXiv:0909.3255 [hep-lat]].
- [72] T. Umeda, Phys. Rev. D **75**, 094502 (2007).
- [73] M. G. Alford, W. Dimm, G. P. Lepage, G. Hockney and P. B. Mackenzie, Phys. Lett. B **361**, 87 (1995) [arXiv:hep-lat/9507010].
- [74] D. B. Kaplan, Phys. Lett. B **288**, 342 (1992); Y. Shamir, Nucl. Phys. **B406**, 90 (1993); Y. Shamir, Phys. Rev. D **59**, 054506 (1999).
- [75] V. Bernard, N. Kaiser, U. G. Meissner, Nucl. Phys. B **357**, 129 (1991).
- [76] G. P. Lepage, in Proceedings of TASI'89 Summer School, edited by T. DeGrand and D. Toussaint (World Scientific, Singapore, 1990), p. 97
- [77] H. -X. Chen and E. Oset, arXiv:1202.2787 [hep-lat].